Available online at www.sciencedirect.com
ScienceDirect
Ocean Engineering 34 (2007) 2074–2085
OCEAN ENGINEERING
www.elsevier.com/locate/oceaneng

Path following control system for a tanker ship model

Lúcia Moreira[a], Thor I. Fossen[b], C. Guedes Soares[a,*]

[a]Unit of Marine Technology and Engineering, Instituto Superior Técnico, Av. Rovisco Pais, 1049-001 Lisboa, Portugal
[b]Centre of Ships and Ocean Structures, Norwegian University of Science and Technology, NO-7491 Trondheim, Norway

Received 4 October 2006; accepted 7 February 2007
Available online 10 April 2007

Abstract

A two-dimensional path following control system for autonomous marine surface vessels is presented. The guidance system is obtained through a way-point guidance scheme based on line-of-sight projection algorithm and the speed controller is achieved through state feedback linearization. A new approach concerning the calculation of a dynamic line-of-sight vector norm is presented which main idea is to improve the speed of the convergence of the vehicle to the desired path. The results obtained are compared with the traditional line-of-sight scheme. It is intended that the complete system will be tested and implemented in a model of the "Esso Osaka" tanker. The results of simulations are presented here showing the effectiveness of the system aiming in to be robust enough to perform tests either in tanks or lakes.

Keywords: Ship steering; Line-of-sight guidance; Manoeuvrability; Control; Simulation results

1. Introduction

The use of autonomous marine vehicles for different applications is growing, because of their low cost compared with full scale and fully manned vessels. Both underwater and surface vehicles are being used for various missions related with oceanography, hydrography, coastal and inland waters monitoring, among others. One of the key aspects that allow such vessels to operate is to have autonomous guidance and control technologies that will allow them to perform predefined missions.

Several techniques can be used for this purpose and it is important to be able to test them in the natural environment. To achieve this objective a ship model has been constructed, representing one ship hull that has been very much studied from a manoeuvring point of view and about which there is a large amount of manoeuvring information. This is the tanker Esso Osaka (see Fig. 1) which, although not being the typical hull of surface autonomous vehicles, will allow different guidance and control strategies to be tested.

In this paper a practical guidance and control system is introduced for the path following of marine surface vehicles. Autonomous guidance and control technologies applied to marine vehicles are recognized as considerably important to the objective of achieving reliable and low-cost vessel operations in the sea, lakes or confined waters. Specifically, marine vehicles equipped with guidance and control systems must be able to navigate in multiple mission or test scenarios. Typically the autonomous vehicles are required to have good manoeuvrability capabilities as well as to be able to keep a desired path, normally in shallow waters and confined spaces under the influence of external disturbances as currents, wind or waves.

In this paper simulations are presented in order to demonstrate the performance of the guidance and control design for the model of the "Esso Osaka" tanker. The whole system will be implemented and ealuated through tests that can be performed in lakes.

Traditionally, trajectory tracking control systems for autonomous vehicles are functionally divided into three subsystems that must be implemented on board the platforms: guidance, navigation and control (Fossen, 2000). Guidance is the action or the system that continuously

*Corresponding author.
E-mail address: guedess@mar.ist.utl.pt (C. Guedes Soares).

0029-8018/$ - see front matter © 2007 Elsevier Ltd. All rights reserved.
doi:10.1016/j.oceaneng.2007.02.005

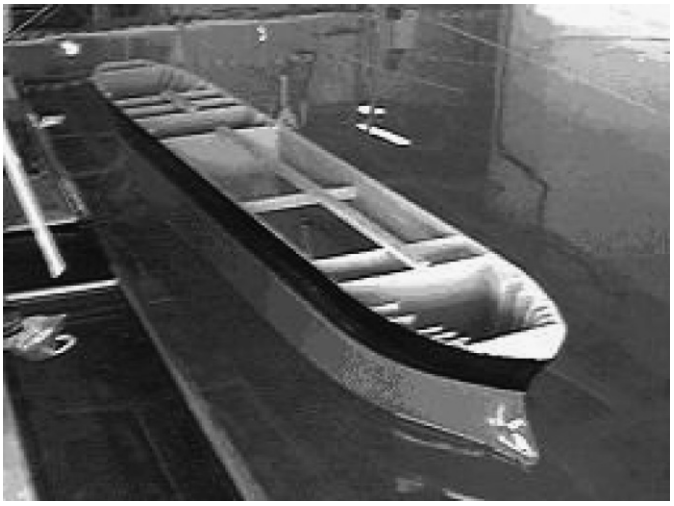

Fig. 1. The "Esso Osaka" model ship.

computes the reference (desired) position, velocity and acceleration of the vehicle to be used by the control system; Navigation is the science of directing a vehicle by determining its position, course, and travelled distance; and finally Control is the action of determining the necessary control forces and moments to be provided by the vehicle in order to satisfy a certain control objective. The desired control objective is usually seen in conjunction with the guidance system. Building the control algorithm involves the design of feedback and feedforward control laws. The outputs from the navigation system, position, velocity and acceleration, are used for feedback control while feedforward control is implemented using signals available in the guidance system and other external sensors.

The solution adopted here was to design a conventional autopilot controlling the heading ψ and a speed controller controlling the vehicle's speed u in combination with a line-of-sight (LOS) algorithm. The way points (trajectory) can be generated using many criteria, usually based on the mission of the vehicle, information about environmental and geographical data (wind, waves, currents, shallow waters islands, etc.), obstacles and collision avoidance (introducing safety margins) and feasibility, meaning that each way point must be feasible, i.e., it must be possible to manoeuvre to the next way point without exceeding maximum speed, turning rate, etc. (Fossen, 2000).

Trajectory tracking control based on LOS for marine surface vessels has been adopted by Fossen et al. (2003) in which a 3 degrees-of-freedom (DOF) (surge, sway, and yaw) nonlinear controller for path following of marine craft is derived using only two controls. In this case the path following is achieved by a geometric assignment based on a LOS projection algorithm for minimization of the cross-track error to the path and the desired speed along the path can be specified independently. Breivik and Fossen (2004a, 2004b) present a guidance-based approach whose main idea is to explicitly control the velocity vector of the vehicles in such a way that they converge to and follow the desired geometrical paths in a natural and elegant manner.

This paper main contribution is the vehicle manoeuvring design based on a way-point guidance algorithm by LOS (Healey and Lienard, 1993), which is used to compute the desired heading angle. A new and different approach concerning the calculation of a dynamic LOS vector norm is presented in order to improve the convergence of the LOS algorithm since it is important to minimize the cross-track error, i.e., the shortest distance between the vehicle and the straight line (Pettersen and Lefeber, 2001). In addition, a tracking controller including a feedforward term and speed controller obtained through state feedback linearization are developed.

To avoid large bumps in the computed desired heading angle and speed and to provide the necessary derivatives to the respective controllers, the commanded LOS heading and model speed are fed through reference models. A PID heading controller is derived and its gains are obtained after simplification of the nonlinear manoeuvring mathematical model of "Esso Osaka" in a 2 DOF (sway–yaw) linear manoeuvring model. This simplified model is just used for this purpose of identification of the heading controller parameters. A feedforward term to achieve accurate and rapid course-changing manoeuvres is also added to this controller. A speed controller is designed through state feedback linearization.

2. "Esso Osaka" modelling

Six independent coordinates are necessary to determine the position and orientation of a rigid body. The first three coordinates and their time derivatives correspond to the position and translational motion along the x-, y-, and z-axes, while the last three coordinates and time derivatives are used to describe orientation and rotational motion. For marine vehicles, the six different motion components are conveniently defined as: surge, sway, heave, roll, pitch and yaw, as can be seen in Table 1.

2.1. Coordinate frames

When analysing the motion of marine vehicles in 6 DOF it is convenient to define two coordinate frames. The moving coordinate frame $X_0Y_0Z_0$ is conveniently fixed to the vehicle and is called the body-fixed reference frame. The origin 0 of the body-fixed frame is usually chosen to coincide with the centre of gravity (CG) when CG is in the principal plane of symmetry or at any other convenient point if this is not the case.

For marine vehicles, the body axes X_0, Y_0 and Z_0 coincide with the principal axes of inertia, and are usually defined as:

X_0—longitudinal axis (directed from aft to fore);
Y_0—transverse axis (directed to starboard);
Z_0—normal axis (directed from top to bottom).

Table 1
Notation used for marine vehicles

DOF	Motion/rotation	Forces/ moments	Linear/ angular velocities	Positions/ euler angles
1	In x-direction (surge)	X	u	x
2	In y-direction (sway)	Y	v	y
3	In z-direction (heave)	Z	w	z
4	About x-axis (roll)	K	p	ϕ
5	About y-axis (pitch)	M	q	θ
6	About z-axis (yaw)	N	r	ψ

The motion of the body-fixed frame is described relative to an inertial reference frame. For marine vehicles it is usually assumed that the accelerations of a point on the surface of the Earth can be neglected. Indeed, this is a good approximation since the motion of the Earth hardly affects low speed marine vehicles. As a result of this, an earth-fixed reference frame XYZ can be considered to be inertial. This suggests that the position and orientation of the vehicle should be described relative to the inertial reference frame while the linear and angular velocities of the vehicle should be expressed in the body-fixed coordinate system. The different quantities are defined according to the SNAME notation (1950), as indicated in Table 1. Based on this notation, the general motion of a marine vehicle in 6 DOF can be described by the following vectors:

$$\eta = \left[\eta_1^{\mathrm{T}}, \eta_2^{\mathrm{T}}\right]^{\mathrm{T}}, \quad \eta_1 = [x, y, z]^{\mathrm{T}}, \quad \eta_2 = [\phi, \theta, \psi]^{\mathrm{T}},$$
$$v = \left[v_1^{\mathrm{T}}, v_2^{\mathrm{T}}\right]^{\mathrm{T}}, \quad v_1 = [u, v, w]^{\mathrm{T}}, \quad v_2 = [p, q, r]^{\mathrm{T}},$$
$$\tau = \left[\tau_1^{\mathrm{T}}, \tau_2^{\mathrm{T}}\right]^{\mathrm{T}}, \quad \tau_1 = [X, Y, Z]^{\mathrm{T}}, \quad \tau_2 = [K, M, N]^{\mathrm{T}}.$$

Here η denotes the position and orientation vector with coordinates in the earth-fixed frame, v denotes the linear and angular velocity vector with coordinates in the body-fixed frame and τ is used to describe the forces and moments acting on the vehicle in the body-fixed frame.

2.2. Froude's scaling law

Hydrodynamic model tests are usually performed according to Froude's scaling law. Froude's law ensures that the correct relationship is kept between inertial and gravitational forces when the full-scale vessel is scaled down to the model dimensions, and is therefore appropriate for model tests involving water waves. Gravitational and inertial forces normally dominate the loading on ships (except for viscous roll damping forces), and Froude scaling is therefore generally adequate (BMT Fluid Mechanics, 2001). Froude's law requires the Froude number, F_n, to be the same at model and full scales:

$$F_n = \frac{U}{\sqrt{gL}}, \tag{1}$$

where L and U are the length and velocity of the ship, respectively, and g is the acceleration due to gravity.

Geometrical scaling is usually used throughout, in order to ensure that correct Froude number scaling is applied to all physical quantities of the ship. This means that all lengths involved in a particular model test are scaled by the same factor. Thus, if the water depth is represented at a scale of 1:k, then so too are the ship's length, breadth and draught, also the wave height and wave length,

A water density correction factor is also normally applied. Model tests are normally performed in freshwater, whereas the full-scale ship will be navigating in salt water. The ratio between standard salt water density and fresh water density, r, is typically 1.025.

Table 2 shows how Froude's scaling law is applied in hydrodynamic model testing to various commonly used physical quantities. k is the scaling factor applied to lengths, and r is the ratio between salt water density and freshwater density. Scaling laws for other quantities may be found by combining relevant mass, length and time dimensions in the appropriate way.

2.3. Process plant model

This section describes the model of the "Esso Osaka" ship. For the simulation and verification of the guidance and control designs, a good mathematical model of the ship is required to generate typical input/output data. The dynamics of the "Esso Osaka" tanker is described by a model based on the horizontal motion with the motion variables of surge, sway and yaw (Abkowitz, 1980).

The model was scaled 1:100 ($k = 100$) from the real "Esso Osaka" ship. The vehicle main characteristics are listed in Table 3 and the nondimensional hydrodynamic coefficients are presented in Table 4. The values of the coefficients are used to simulate the "Esso Osaka" trial manoeuvres.

Table 2
Froude scaling of various physical quantities

Quantity	Typical units	Scaling parameter
Length	m	k
Time	s	$k^{1/2}$
Frequency	1/s	$k^{-1/2}$
Velocity	m/s	$k^{1/2}$
Acceleration	m/s^2	1
Volume	m^3	k^3
Water density	ton/m^3	r
Mass	ton	rk^3
Force	kN	rk^3
Moment	kN m	rk^4
Extension stiffness	kN/m	rk^2

Table 3
"Esso Osaka" model particulars

"Esso Osaka" model	
Length overall	3.430 m
Length between perpendiculars	3.250 m
Breadth	0.530 m
Draft (estimated at trials)	0.217 m
Block coefficient	0.831
Number of rudders	1
Displacement (estimated at trials)	319.40 kg
Rudder area	0.0120 m^2
Propeller area	0.0065 m^2
Longitudinal CG (fw of midship)	0.103 m

Table 4
"Esso Osaka" nondimensional hydrodynamic coefficients

Coefficient	Value	Coefficient	Value
$(m - Y_{\dot{v}})'$	0.0352	Y'_{vrr}	0.00611
$(I_z - N_{\dot{r}})'$	0.00222	X'_{ee}	−0.00224
Y'_v	−0.0261	X'_{rrvv}	−0.00715
Y'_r	0.00365	N'_{eee}	0.00116
N'_v	−0.0105	Y'_{vrr}	−0.0450
Y'_r	−0.00480	η'_1	-0.962×10^{-5}
Y'_δ	−0.00283	η'_2	-0.446×10^{-5}
$X'_{vy} + m'$	0.0266	η'_3	0.0309×10^{-5}
N'_0	−0.00028	m'	0.0181
		C'_R	0.00226

The form of the simulation equations given in this section is the one presented in Abkowitz (1980), where δ is the rudder deflection; m is the ship's mass; I_z is the yaw moment of inertia; x_G is the location of the CG relative to midship; Δu is the change in forward speed (negative Δu is a speed loss); and X, Y and N with subscripts u, v, r and δ are the hydrodynamic coefficients, such as N_v.

Realism calls for accepting the possibility of wind, current and waves during the model operation. As "Esso Osaka" has relatively little abovewater structure, a mild to moderate wind would not cause substantial external excitation. However, even moderate currents could produce substantial external forces on the hull, especially when the current velocity becomes a reasonable fraction of the components of the model ship's speed during the manoeuvre. Because the hydrodynamic forces acting on the model are a function of the relative velocity between the vehicle minus the spatial velocity of the water, the excitation caused by the current in the longitudinal direction and in the transverse direction, x-axis and y-axis, respectively, acting on the appropriate ship coefficients, such as X_u, Y_v and N_v. If u_c is the current's magnitude, α the current's spatial direction (heading), ψ the ship's heading angle, u the ship's spatial forward component of velocity over the ground, and v the ship's spatial transverse component of velocity, the forward component of relative velocity u_r and the transverse component of relative velocity v_r are given by

$$u_r = u - u_c \cos(\psi - \alpha), \tag{2}$$

$$v_r = v + u_c \sin(\psi - \alpha) \tag{3}$$

and the resulting advance speed of the vehicle is given by

$$U_r = \sqrt{u_r^2 + v_r^2}. \tag{4}$$

In the simulation equations, presented from (5) up to (16), the nondimensional form of the coefficients is indicated by a prime marking, that is, η'_1 is the nondimensional form of η_1, etc. The velocities u and v with subscript r refer to the relative velocity between the ship and the water and thereby include the effect of water currents on the forces. This simulation model was validated with real data in Abkowitz (1980) and shown to be a good formulation for the "Esso Osaka" and ships of its type.

The derivatives with respect to time of u and v are given by the following expressions:

$$\dot{u} = \dot{u}_r - u_c r \sin(\psi - \alpha), \tag{5}$$

$$\dot{v} = \dot{v}_r - u_c r \cos(\psi - \alpha) \tag{6}$$

with the derivatives with respect to time of u_r, v_r and r given by

$$\dot{u}_r = \frac{f_1}{m - X_{\dot{u}_r}}, \tag{7}$$

$$\dot{v}_r = \frac{1}{f_4}\left[(I_z - N_{\dot{r}})f_2 - (mx_G - Y_{\dot{r}})f_3\right], \tag{8}$$

$$\dot{r} = \frac{1}{f_4}\left[(m - Y_{\dot{v}_r})f_3 - (mx_G - N_{\dot{v}_r})f_2\right], \tag{9}$$

where

$$\begin{aligned} f_1 = {} & \eta'_1\left[\frac{\rho}{2}L^2\right]u_r^2 + \eta'_2\left[\frac{\rho}{2}L^3\right]mu_r + \eta'_3\left[\frac{\rho}{2}L^4\right]n^2 \\ & - C'_R\left[\frac{\rho}{2}Su_r^2\right] + X'^2_{v_r}\left[\frac{\rho}{2}L^2\right]v_r^2 + X'_{e^2}\left[\frac{\rho}{2}L^2c^2\right]e^2 \\ & + \cdots + \left(X'_{r^2} + m'x'_G\right)\left[\frac{\rho}{2}L^4\right]r^2 \\ & + \left(X'_{v_r r} + m'\right)\left[\frac{\rho}{2}L^3\right]v_r r + X'_{v_r^2 r^2}\left[\frac{\rho}{2}L^4U^{-2}\right]v_r^2 r^2, \end{aligned} \tag{10}$$

$$\begin{aligned} f_2 = {} & Y'_0\left[\frac{\rho}{2}L^2\left(\frac{u_{A\infty}}{2}\right)^2\right] + \left\{Y'_{v_r}\left[\frac{\rho}{2}L^2U_r\right]v_r\right. \\ & \left. + Y'_\delta(c - c_0)\frac{\rho}{2}L^2v_r\right\} + \left\{\left(Y'_r - m'u'_r\right)\left[\frac{\rho}{2}L^3U_r\right]r\right. \\ & \left. - \cdots - \frac{Y'_\delta}{2}(c - c_0)\frac{\rho}{2}L^3r\right\} + Y'_\delta\left[\frac{\rho}{2}L^2c^2\right]\delta \\ & + Y'_{r^2v_r}\left[\frac{\rho}{2}L^4U_r^{-1}\right]r^2v_r + Y'_{e^3}\left[\frac{\rho}{2}L^2c^2\right]e^3, \end{aligned} \tag{11}$$

$$f_3 = N'_0\left[\frac{\rho}{2}L^3\left(\frac{u_{A\infty}}{2}\right)^2\right] + \left\{N'_{v_r}\left[\frac{\rho}{2}L^3U_r\right]v_r - N'_\delta(c-c_0)\frac{\rho}{2}L^3v_r\right\} \times \left\{\left(N'_r - m'x'_G u'_r\right)\left[\frac{\rho}{2}L^4U_r\right]r + \cdots + \frac{1}{2}N'_\delta(c-c_0)\frac{\rho}{2}L^4r\right\} + N'_\delta\left[\frac{\rho}{2}L^3c^2\right]\delta + N'_{r^2v_r}\left[\frac{\rho}{2}L^5U_r^{-1}\right]r^2v_r + N'_{e^3}\left[\frac{\rho}{2}L^3c^2\right]e^3, \quad (12)$$

$$f_4 = \left(m' - Y'_{\dot v_r}\right)\left[\frac{\rho}{2}L^3\right]\left(I'_z - N'_{\dot r}\right)\left[\frac{\rho}{2}L^5\right] - \left(m'x'_G - N'_{\dot v_r}\right)\left[\frac{\rho}{2}L^4\right]\left(m'x'_G - Y'_{\dot r}\right)\left[\frac{\rho}{2}L^4\right], \quad (13)$$

where ρ is the mass density of water; L is the length of the ship between perpendiculars; n are the propeller rps; C_R is the resistance coefficient of the vehicle (including the drag of windmilling propeller); S is the wetted surface area of the ship; and c is the weighted average flow speed over rudder given by

$$c = \sqrt{\frac{A_P}{A_R}[(1-w)u_r + ku_{A\infty}]^2 + \frac{A_R - A_P}{A_R}(1-w)^2u_r^2}. \quad (14)$$

c_0 is the value of c when the propeller rotational speed and ship forward speed are in equilibrium in straight-ahead motion (when $u = u_0$ and $n = n_0$); A_P is the propeller area; A_R is the rudder area; w is the wake fraction; $u_{A\infty}$ is the induced axial velocity behind the propeller disk given by

$$u_{A\infty} = -(1-w)u + \sqrt{(1-w)^2u^2 + \frac{8}{\pi}K_T(nD)^2}. \quad (15)$$

At a general position x, the induced mean axial velocity u_A is acquired by multiplying $u_{A\infty}$ by the factor k, which is a function of the axial distance x from the propeller disk to the point of interest. In this case x is the location of the quarter mean chord of the rudder and an infinite-blade propeller is used to find the functional relationship between k and x (Abkowitz, 1980). K_T is the propulsive coefficient; D is the propeller diameter; and e is the effective rudder angle given by

$$e = \delta\frac{v}{c} + \frac{rL}{2c}. \quad (16)$$

Despite the high nonlinearities contained in the ship's rudder dynamics it is possible to model it, in an approximated linear form, as a first order system given by

$$\delta(s) = \frac{1}{1+T_Ls}\delta_c(s), \quad (17)$$

where δ is the rudder angle, δ_c is the order of rudder angle and T_L is the time constant, which value usually varies from 3 to 5 s in a full-scale ship (Moreira and Guedes Soares, 2003). For this purpose T_L is considered equal to 0.5 s for the model. This approximation is valid because only low frequency signals are considered.

2.4. Control plant model

In order to design the steering autopilot becomes necessary to simplify the mathematical model described in the previous section in a 2 DOF (sway–yaw) linear manoeuvring model. This simplified model should contain only the main physical properties of the process.

A linear manoeuvring model is based on the assumption that the cruise speed of the ship u is kept constant ($u = u_0 \approx$ constant) while v and r are assumed to be small. A 2 DOF nonlinear manoeuvring model can be expressed by

$$\mathbf{M}\dot v + \mathbf{C}(v)v + \mathbf{D}(v)v = \tau, \quad (18)$$

where $\mathbf{M}$ is the system inertia matrix, $\mathbf{C}(v)$ is the Coriolis-centripetal matrix, $\mathbf{D}(v)$ is the damping matrix, τ is the vector of control inputs and $v = [v, r]^T$ is the sway and yaw state vector. $\mathbf{C}(v)v$ can be represented by

$$\mathbf{C}(v)v = \begin{bmatrix} (m - X_{\dot u})u_0 r \\ (m - Y_{\dot v})u_0 v + (mx_G - Y_{\dot r})u_0 r - (m - X_{\dot u})u_0 v \end{bmatrix} = \begin{bmatrix} 0 & (m - X_{\dot u})u_0 \\ (X_{\dot u} - Y_{\dot v})u_0 & (mx_G - Y_{\dot r})u_0 \end{bmatrix}\begin{bmatrix} v \\ r \end{bmatrix} \quad (19)$$

and as the ship will be controlled by a single rudder

$$\boldsymbol{\tau} = \boldsymbol{b}\delta = \begin{bmatrix} -Y_\delta \\ -N_\delta \end{bmatrix}\delta, \quad (20)$$

where δ is the rudder angle.

It is convenient to write total hydrodynamic damping as

$$\mathbf{D}(v) = \mathbf{D} + \mathbf{D}_n(v) \approx \mathbf{D}, \quad (21)$$

where $\mathbf{D}$ is the linear damping matrix and $\mathbf{D}_n(v)$ is the nonlinear damping matrix that is neglected in this representation.

The resulting model then becomes

$$\mathbf{M}\dot v + \mathbf{N}(u_0)v = \boldsymbol{b}\delta. \quad (22)$$

with

$$\mathbf{M} = \begin{bmatrix} m - Y_{\dot v} & mx_G - Y_{\dot r} \\ mx_G - Y_{\dot r} & I_z - N_{\dot r} \end{bmatrix}, \quad (23)$$

$$\mathbf{N}(u_0) = \begin{bmatrix} -Y_v & (m - X_{\dot u})u_0 - Y_r \\ (X_{\dot u} - Y_{\dot v})u_0 - N_v & (mx_G - Y_{\dot r})u_0 - N_r \end{bmatrix}, \quad (24)$$

$$\boldsymbol{b} = \begin{bmatrix} -Y_\delta \\ -N_\delta \end{bmatrix}. \quad (25)$$

Nomoto et al. (1957) proposed a linear model for the ship steering equations that is obtained by eliminating the sway velocity from (22). The resulting model is named the Nomoto's second order model and is given by a simple

transfer function between r and δ:

$$\frac{r}{\delta}(s) = \frac{K(1+T_3 s)}{(1+T_1 s)(1+T_2 s)}, \tag{26}$$

where T_i ($i = 1, 2, 3$) are time constants and K is the gain constant.

A first order approximation to (26) is obtained by defining the *effective time constant*:

$$T = T_1 + T_2 - T_3 \tag{27}$$

such that

$$\frac{r}{\delta}(s) = \frac{K}{(1+Ts)}, \tag{28}$$

where T and K are known as the Nomoto time and gain constants, respectively. Neglecting the roll and pitch modes ($\phi = \theta = 0$) such that

$$\dot{\psi} = r \tag{29}$$

finally yields

$$\frac{\psi}{\delta}(s) = \frac{K(1+T_3 s)}{s(1+T_1 s)(1+T_2 s)} \approx \frac{K}{s(1+Ts)}. \tag{30}$$

This model is widely used for ship autopilot design due to its compromise between simplicity and accuracy.

Journée (2001) and Clarke (2003) showed that the first order Nomoto equation can be used to analyse the ship behaviour during zigzag manoeuvres, to find the values of K and T. If the equation of motion given by

$$T\dot{r} + r = K\delta \tag{31}$$

is integrated with respect to time t, the following equation results,

$$T\int_0^t \dot{r}\,\mathrm{d}t + \int_0^t r\,\mathrm{d}t = K\int_0^t \delta\,\mathrm{d}t. \tag{32}$$

The left-hand side can be integrated to give the following:

$$T[r]_o^t + [\psi]_o^t = K\int_0^t \delta\,\mathrm{d}t. \tag{33}$$

Applying (33) to the first two heading overshoots of the zigzag manoeuvre, as shown in Fig. 2, where the shaded area gives the integral term and at points delimited by the crosses (1 and 2), the yaw rate r is equal to zero. The term K is found immediately from the following expression:

$$K = -\frac{\psi_1 - \psi_2}{\int_{t_1}^{t_2} \delta\,\mathrm{d}t}. \tag{34}$$

Similarly, (33) is applied to the first two zero crossing points of the heading record of the zigzag manoeuvre, as shown in Fig. 3, where again the integral term is given by the shaded area.

In this case, at the two points delimited by the crosses (3 and 4), the heading ψ is equal to zero and T may be calculated from

$$\frac{K}{T} = -\frac{r_3 - r_4}{\int_{t_3}^{t_4} \delta\,\mathrm{d}t}. \tag{35}$$

The values obtained for K and T of the first order Nomoto model, considering a speed u_0 equal to 0.4 m/s, are:

$K = 0.1705\,\mathrm{s}^{-1}$,

$T = 7.1167\,\mathrm{s}$,

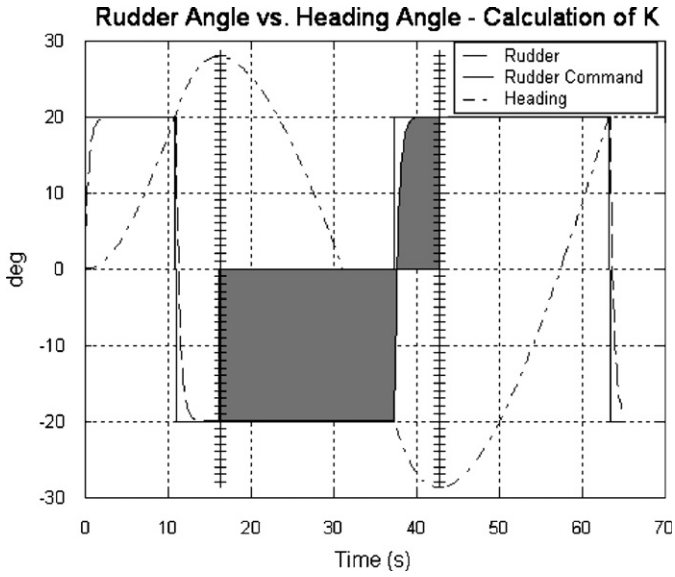

Fig. 2. Derivation of K from 20-20 zigzag manoeuvre.

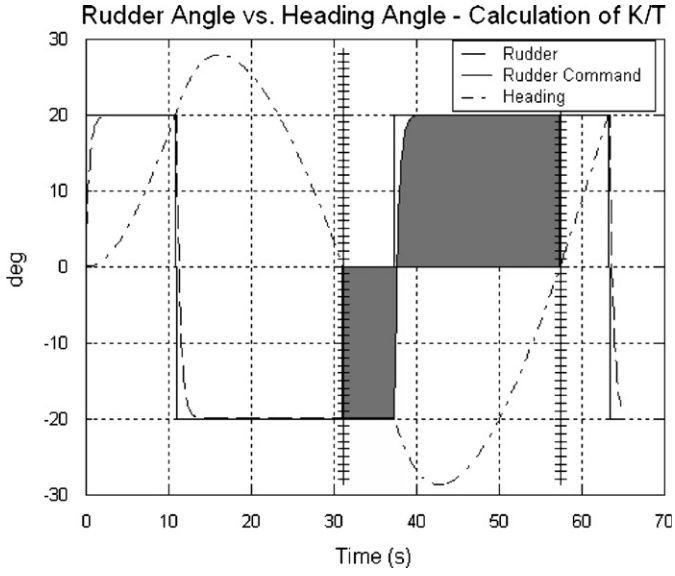

Fig. 3. Derivation of K/T from 20-20 zigzag manoeuvre.

3. PID heading controller

This section describes the design of the PID heading controller. The main goal in this design is to calculate the

controller gains in terms of the Nomoto constants obtained in the previous section and introduce them in the PID controller law. After this a reference model and a feedforward term will be added to the controller in order to achieve more accurate and rapid course-changing manoeuvres.

3.1. PID controller

Assuming that ψ is measured by using a compass, a PID-controller is (Fossen, 2000):

$$\tau_N(s) = \tau_{PID}(s) = -K_p\left(1 + T_d s + \frac{1}{T_i s}\right)\tilde{\psi}(s), \tag{36}$$

where τ_N is the controller yaw moment, $\tilde{\psi} = \psi - \psi_d$ is the heading error and K_p (>0) is the proportional gain constant, T_d (>0) is the derivative time constant, and T_i (>0) is the integral time constant. A continuous-time representation of the controller is

$$\tau_{PID}(t) = -K_p\tilde{\psi} - K_d\tilde{r} - K_i\int_0^t \tilde{\psi}(\tau)\,d\tau, \tag{37}$$

where $\tilde{r} = r - r_d$, $K_d = K_p T_d$, and $K_i = K_p T_i$. The controller gains can be found by pole placement in terms of the design parameters ω_n and ζ, through:

$$K_p = \frac{\omega_n^2 T}{K} > 0,$$
$$K_d = \frac{2\zeta\omega_n T - 1}{K} > 0,$$
$$K_i = \frac{\omega_n^3 T}{10K} > 0,$$

where ω_n is the natural frequency and ζ is the relative damping ratio of the first order system. In this case was considered $\omega_n = 1$ rad/s and critical damping with $\zeta = 1$. Thus, the following controller gains are obtained:

$$K_p = 41.7422,$$
$$K_d = 77.6189,$$
$$K_i = 0.0587.$$

3.2. Autopilot reference model

An autopilot must have both course-keeping and turning capabilities. This can be obtained in one design by using a reference model to compute the desired states ψ_d, r_d, and $\dot{r}_d$ needed for course-changing (turning) wile course-keeping, that is

$$\psi_d = \text{constant} \tag{38}$$

can be treated as a special case of turning. A simple third-order filter for this purpose is

$$\frac{\psi_d}{\psi_r}(s) = \frac{\omega_n^3}{(s+\omega_n)(s^2 + 2\zeta\omega_n s + \omega_n^2)}, \tag{39}$$

where the reference ψ_r is the operator input, ζ is the relative damping ratio, and ω_n is the natural frequency. Notice that

$$\lim_{t\to\infty} \psi_d(t) = \psi_r \tag{40}$$

and that $\dot{\psi}_d$ and $\ddot{\psi}_d$ are smooth and bounded for steps in ψ_r. This is the main motivation for choosing a third-order model. In this case $\omega_n = 0.45$ rad/s and critical damping $\zeta = 1$ were considered.

3.3. Feedforward term

A feedforward term to achieve accurate and rapid course-changing manoeuvres can be added to the controller. Assuming that both ψ and r are measured by a compass and a rate gyro the PID-controller for full state feedback is given by

$$\tau_N(s) = \tau_{FF}(s) - K_p\left(1 + T_d s + \frac{1}{T_i s}\right)\tilde{\psi}(s), \tag{41}$$

where τ_{FF} is a feedforward term to be decided.

The feedforward term τ_{FF} in Eq. (41) is determined such that perfect tracking during course-changing manoeuvres is obtained. Using Nomoto's first-order model as basis for feedforward, suggests that reference feedforward should be included according to

$$\tau_{FF} = \frac{T}{K}\dot{r}_d + \frac{1}{K}r_d. \tag{42}$$

4. Speed controller using state feedback linearization

The basic idea with feedback linearization is to transform the nonlinear systems dynamics into a linear system. Conventional control techniques like pole placement and linear quadratic optimal control theory can then be applied to the linear system (Fossen, 2000).

Combining Eqs. (5) and (7) the model of the ship in surge is given by

$$\dot{u} = \frac{f_1}{m - X_{\dot{u}_r}} - u_c r\sin(\psi - \alpha) \tag{43}$$

with

$$f_1 = \text{Thrust}(u_r, n) + f_1^*(u_r, v_r, u, v, r, \delta). \tag{44}$$

The thrust term is given by

$$\text{Thrust}(u_r, n) = \eta_1'\left[\frac{\rho}{2}L^2\right]u_r^2 + \eta_2'\left[\frac{\rho}{2}L^3\right]nu_r + \eta_3'\left[\frac{\rho}{2}L^4\right]n^2 \tag{45}$$

and f_1^* is given by

$$f_1^*(u_r, v_r, u, v, r, \delta) = -C'_R\left[\frac{\rho}{2}Su_r^2\right] + X'^2_{v_r}\left[\frac{\rho}{2}L^2\right]v_r^2 + X'_{e^2}\left[\frac{\rho}{2}L^2c^2\right]e^2 + \cdots$$

$$+\left(X'_{r^2}+m'x'_{\mathrm{G}}\right)\left[\frac{\rho}{2}L^4\right]r^2 + \left(X'_{v_{\mathrm{r}}r}+m'\right)\left[\frac{\rho}{2}L^3\right]v_{\mathrm{r}}r + X'_{v_{\mathrm{r}}^2r^2}\left[\frac{\rho}{2}L^4U^{-2}\right]v_{\mathrm{r}}^2r^2. \quad (46)$$

The commanded acceleration can be calculated through (Fossen, 2000)

$$a^b = \dot{u}_{\mathrm{d}} - K_{\mathrm{p}}(u_{\mathrm{r}}-u_{\mathrm{d}}) - K_{\mathrm{i}}\int_0^t (u_{\mathrm{r}}-u_{\mathrm{d}})\,\mathrm{d}\tau. \quad (47)$$

Thus, the speed controller can be computed by

$$\tau_{\mathrm{Thrust}} = \left(m - X_{\dot{u}_{\mathrm{r}}}\right)\left[\dot{u}_{\mathrm{d}} - K_{\mathrm{p}}(u_{\mathrm{r}}-u_{\mathrm{d}}) - K_{\mathrm{i}}\int_0^t (u_{\mathrm{r}}-u_{\mathrm{d}})\,\mathrm{d}\tau + u_{\mathrm{c}}r\sin(\psi-\alpha)\right] - f_1^*(u_{\mathrm{r}},v_{\mathrm{r}},u,v,r,\delta). \quad (48)$$

The following controller gains are used:

$K_{\mathrm{p}} = 0.15,$

$K_{\mathrm{i}} = 1e-5.$

A second-order filter for this purpose is

$$\frac{u_{\mathrm{d}}}{r^b}(s) = \frac{\omega^2}{s^2+2\zeta\omega_{\mathrm{n}}s+\omega^2}, \quad (49)$$

where $\zeta>0$ and $\omega>0$ are the reference model damping ratio and natural frequency while r^b is the commanded input (desired surge speed). In this case was considered $\omega_{\mathrm{n}} = 0.25\,\mathrm{rad/s}$ and critical damping with $\zeta = 1$.

5. LOS guidance

Systems for guidance are systems consisting of a way-point generator with human interface. One solution to design this system is to store the selected way points in a way-point database and use them to generate a trajectory (path) for the ship. Other systems can be linked to this way-point guidance system as the case of weather routing, collision and obstacle avoidance, mission planning, etc. (Fossen, 2000). In combination with these systems a widely used method for path control is LOS guidance. LOS schemes have been applied to surface ships by McGookin et al. (1998) and Fossen et al. (2003). In this methodology it is computed a LOS vector from the ship to the next way point (or a point on the path between two way points) for heading control. If the ship has a course autopilot the angle between the LOS vector and the predescribed path can be used as a set-point for the autopilot, forcing the ship to track the path (Fossen, 2000).

When moving along the path a switching mechanism for selecting the next way point is needed. The way point (x_{k+1}, y_{k+1}) can be selected on a basis of whether the ship lies within a circle of acceptance with radius R_0 around the way point (x_k, y_k). In many applications the LOS vector is taken as a vector from the body-fixed origin (x, y) to the next way point (x_k, y_k). This suggests that the set-point to the course autopilot should be chosen as

$$\psi_{\mathrm{d}}(t) = a\tan2\big(y_k - y(t), x_k - x(t)\big), \quad (50)$$

where (x, y) is the ship position measurement. The four quadrant inverse tangent function $a\tan 2\,(y, x)$ is used to ensure that

$$-\pi \leqslant a\tan 2(y,x) \leq \pi. \quad (51)$$

The reference model given in Section 3.2 will generate the necessary signals required by the heading controller as well as smoothing the discontinuous way-point switching to prevent rapid changes in the desired yaw angle fed to the controller. However, since the a tan 2-function is discontinuous at the $-\pi/\pi$ junction, the reference model cannot be applied directly to its output. This is solved by constructing a mapping ψ_{d}: $\langle -\pi, \pi\rangle \rightarrow \langle -\infty, \infty\rangle$ and sandwiching the reference filter between ψ_{d} and ψ_{d}^{-1}. Details about the mappings can be found in Breivik (2003).

The drawback with a LOS vector pointing to the next way point is that a way point located far away from the ship will result in large cross-track errors in the presence of wind, current and wave disturbances. Therefore, the LOS vector can be defined as the vector from the vessel coordinate origin (x, y) to the intersecting point on the path $(x_{\mathrm{los}}, y_{\mathrm{los}})$ a distance n ship lengths L_{pp} ahead of the vessel. Thus, the desired yaw angle can be computed as

$$\psi_{\mathrm{d}}(t) = a\tan 2\big(y_{\mathrm{los}} - y(t), x_{\mathrm{los}} - x(t)\big), \quad (52)$$

where the LOS coordinates $(x_{\mathrm{los}}, y_{\mathrm{los}})$ are given by

$$\big(y_{\mathrm{los}} - y(t)\big)^2 + \big(x_{\mathrm{los}} - x(t)\big)^2 = \big(nL_{\mathrm{pp}}\big)^2, \quad (53)$$

$$\left(\frac{y_{\mathrm{los}} - y_{k-1}}{x_{\mathrm{los}} - x_{k-1}}\right) = \left(\frac{y_k - y_{k-1}}{x_k - x_{k-1}}\right) = \text{constant}. \quad (54)$$

Eq. (53) is recognized as the theorem of *Pythagoras* while (54) states that the slope of the path between the way points (x_{k-1}, y_{k-1}) and (x_k, y_k) is constant. Hence, the pair $(x_{\mathrm{los}}, y_{\mathrm{los}})$ can be solved from these two last equations. When moving along the path a switching mechanism for selecting the next way point is needed. Way point (x_{k+1}, y_{k+1}) can be selected on a basis of whether the ship lies within a *circle of acceptance* with radius R_0 around way point (x_k, y_k). Moreover, if the vehicle positions $(x(t), y(t))$ at time t satisfies:

$$[x_k - x(t)]^2 + \big[y_k - y(t)\big]^2 \leqslant R_0^2 \quad (55)$$

the next way point (x_{k+1}, y_{k+1}) should be selected, i.e., k should be incremented to $k = k+1$. A guideline can be to choose R_0 equal to two ship lengths, that is $R_0 = 2L_{\mathrm{pp}}$ (Fossen, 2000).

5.1. LOS—alternative method using dynamic circle

A new approach is used to improve the convergence of the LOS algorithm through the assumption that the distance n ahead of the vessel instead of be constant will

follow the dynamics given below between two consecutive way points

$$\dot{n}(t) = -K.n(t) \quad \text{for } t \in [t_{k-1}, t_k], \tag{56}$$

where $n(t_{k-1}) = n$ is the initial condition of the differential Eq. (56), K is a design constant parameter to be adjusted and t_k is the instant at the way point k is reached:

$$\left(y_{\text{los}} - y(t)\right)^2 + \left(x_{\text{los}} - x(t)\right)^2 = \left(n(t)L_{\text{pp}}\right)^2. \tag{57}$$

5.2. LOS—alternative method using minimum dynamic circle

Based on the idea presented in the previous section, in this second approach the main objective is to find the minimum circle, i.e., the minimum radius of the circle of the second term of Eq. (57) in order to improve the convergence of the LOS algorithm. Fig. 4 illustrates the principle to achieve the minimum radius to solve the LOS equations.

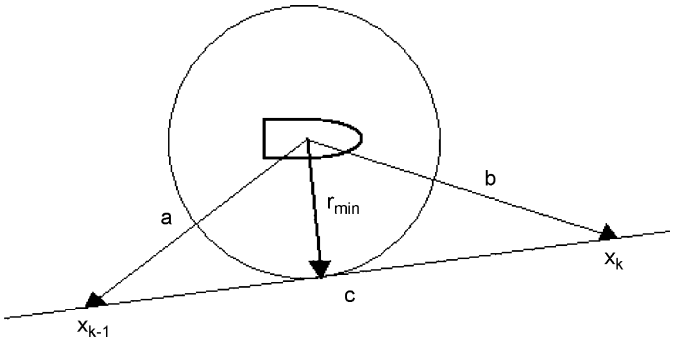

Fig. 4. Geometry to obtain the minimum circle.

The parameters shown in Fig. 4 are given by

$$a(t) = \sqrt{(x(t) - x_{k-1})^2 + \left(y(t) - y_{k-1}\right)^2}, \tag{58}$$

$$b(t) = \sqrt{(x_k - x(t))^2 + \left(y_k - y(t)\right)^2}, \tag{59}$$

$$c(t) = \sqrt{(x_k - x_{k-1})^2 + \left(y_k - y_{k-1}\right)^2}, \tag{60}$$

$$r_{\min}(t) = \sqrt{a(t)^2 - \left(\frac{c(t)^2 - b(t)^2 + a(t)^2}{2c(t)}\right)^2}. \tag{61}$$

Eq. (61) provides the minimum circle according with Fig. 4 but doesn't behave well as $b \to 0$ and $a \to c$. To avoid $r_{\min} \to 0$ it is assumed that

$$n(t)L_{\text{pp}} = r_{\min}(t) + L_{\text{pp}} \tag{62}$$

that is equivalent to assume that n is higher than 1, i.e., $r_{\min} > L_{\text{pp}}$. Thus, the LOS coordinates (x_{los}, y_{los}) are now given by

$$\left(y_{\text{los}} - y(t)\right)^2 + \left(x_{\text{los}} - x(t)\right)^2 = \left(r_{\min}(t) + L_{\text{pp}}\right)^2. \tag{63}$$

6. Case study: Simulation results

In this section case studies will be presented to allow comparing the trajectories based on the LOS coordinates given in Eq. (53) using a constant circle (first method), with the trajectories computed through Eq. (63) using a minimum dynamic circle (second method). These two

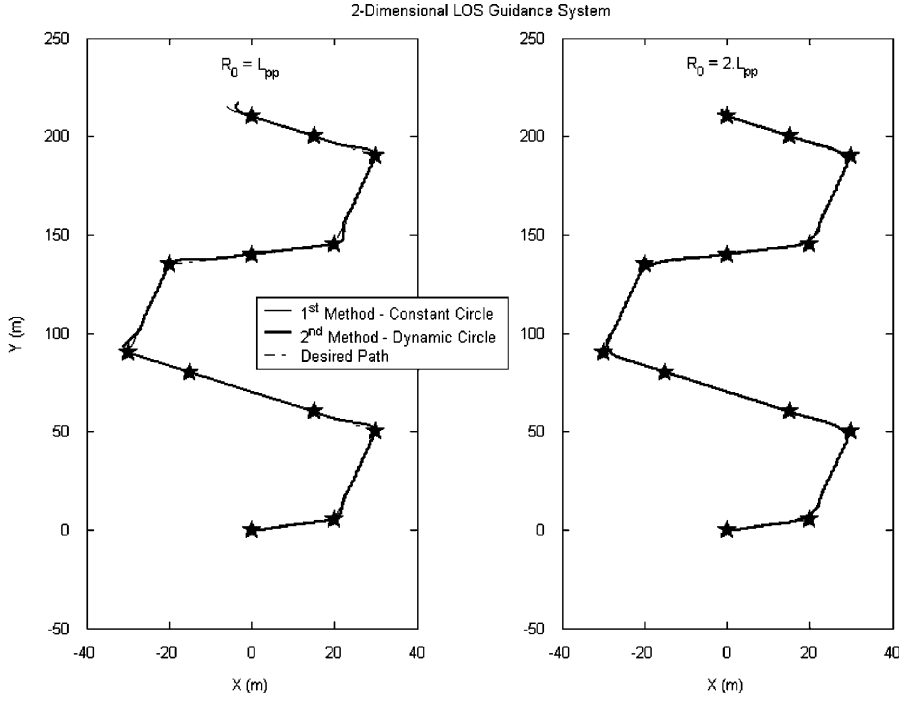

Fig. 5. xy-plot of the simulated and desired geometrical path for $R_0 = L_{\text{pp}}$ and $R_0 = 2L_{\text{pp}}$.

methodologies are compared for two different radius of acceptance: $R_0 = L_{pp} = 3.25\,m$ and $R_0 = 2L_{pp} = 6.50\,m$. All the trajectory tests will be performed in the scale of the model.

The first, second and third desired paths will consist of a total of 12, 10 and 9 way points, respectively:

First trajectory:

$Wpt_1 = (0, 0)\,m$, $Wpt_2 = (20, 5)\,m$, $Wpt_3 = (30, 50)\,m$,
$Wpt_4 = (15, 60)\,m$, $Wpt_5 = (-15, 80)\,m$, $Wpt_6 = (-30, 90)\,m$,
$Wpt_7 = (-20, 135)\,m$, $Wpt_8 = (0, 140)\,m$, $Wpt_9 = (20, 145)\,m$,
$Wpt_{10} = (30, 190)\,m$, $Wpt_{11} = (15, 200)\,m$, $Wpt_{12} = (0, 210)\,m$,

Second trajectory:

$Wpt_1 = (0, 0)\,m$, $Wpt_2 = (20, 5)\,m$, $Wpt_3 = (30, 50)\,m$,
$Wpt_4 = (-30, 95)\,m$, $Wpt_5 = (0, 140)\,m$, $Wpt_6 = (-30, 150)\,m$,
$Wpt_7 = (20, 195)\,m$, $Wpt_8 = (0, 90)\,m$, $Wpt_9 = (0, 45)\,m$,
$Wpt_{10} = (0, 0)\,m$.

Third trajectory:

$Wpt_1 = (0, 0)\,m$, $Wpt_2 = (20, 10)\,m$, $Wpt_3 = (-20, 10)\,m$,
$Wpt_4 = (-25, 20)\,m$, $Wpt_5 = (25, 60)\,m$, $Wpt_6 = (20, 70)\,m$,
$Wpt_7 = (0, 80)\,m$, $Wpt_8 = (-20, 70)\,m$, $Wpt_9 = (0, 70)\,m$.

The ship's initial states for all the trajectories are

$$(x_0, y_0, \psi_0) = (0\,m,\ 0\,m,\ 0\,rad),$$
$$(u_0, v_0, r_0) = (0.41\,m/s,\ 0\,m/s,\ 0\,rad/s).$$

The desired speed is kept constant along the first trajectory with a value of 0.33 m/s, that corresponds to a Froude number F_n equal to 0.0584. For the second and third paths the desired speed will be considered as follows:

$$r^b = \begin{cases} 0.21\,m/s\ (Fn = 0.0372) & \text{if } t_1 \leqslant t < t_2, \\ 0.33\,m/s\ (Fn = 0.0584) & \text{if } t_2 \leqslant t < t_3, \\ 0.66\,m/s\ (Fn = 0.1169) & \text{if } t_3 \leqslant t < t_5, \\ 0.48\,m/s\ (Fn = 0.0850) & \text{if } t_5 \leqslant t < t_9, \\ 0.41\,m/s\ (Fn = 0.0726) & \text{if } t_9 \leqslant t < t_{10}, \end{cases}$$

for the second trajectory,

and

$$r^b = \begin{cases} 0.21\,m/s\ (Fn = 0.0372) & \text{if } t_1 \leqslant t \leqslant t_3, \\ 0.43\,m/s\ (Fn = 0.0762) & \text{if } t_3 < t \leqslant t_6 \\ 0.27\,m/s\ (Fn = 0.0478) & \text{if } t_6 < t \leqslant t_9. \end{cases}$$

for the third trajectory,

Between way points the distance n ahead of the vessel was assumed equal to 3 using the first method (i.e. the constant circle). In the first set of simulations for the first trajectory the radius of acceptance for all way points was set to one ship length ($R_0 = L_{pp}$) and in the second was set to two ship lengths ($R_0 = 2L_{pp}$). Fig. 5 shows a *xy*-plot of the first trajectory simulations of the "Esso Osaka" model position together with the desired geometrical path

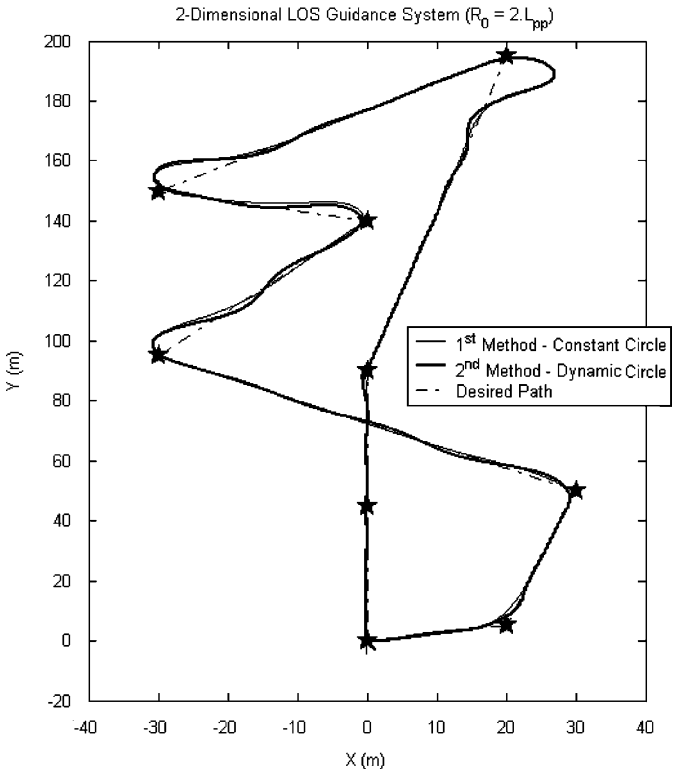

Fig. 6. *xy*-plot of the simulated and desired geometrical path of the second trajectory using the two different methods.

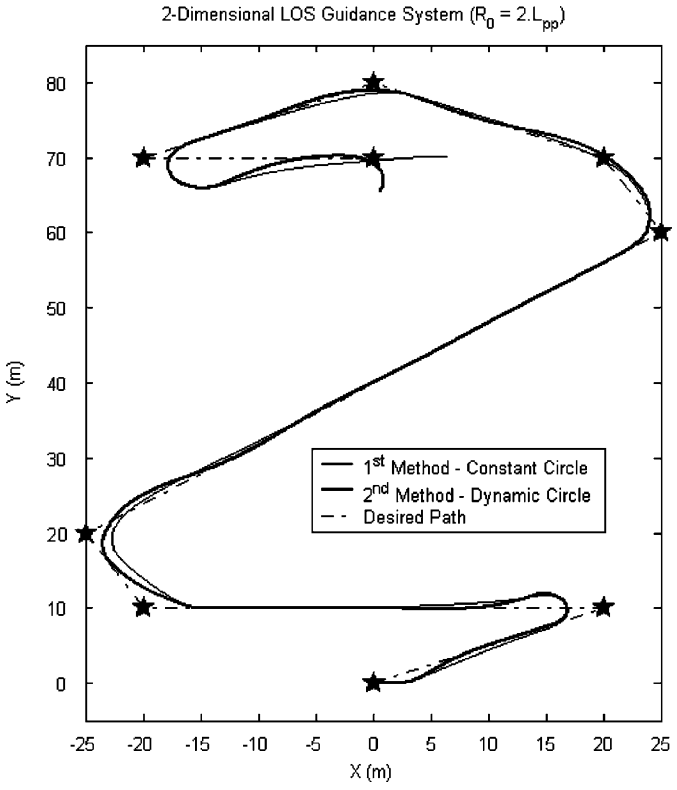

Fig. 7. *xy*-plot of the simulated and desired geometrical path of the third trajectory using the two different methods.

consisting of straight line segments for the two different methods using the radius of acceptance equal to one and two ship lengths.

Figs. 6 and 7 show the *xy*-plots of the simulation of the second and third trajectories, respectively. In these simulations a radius of acceptance equal to two ship lengths was considered.

Figs. 8 and 9 present the errors obtained through the difference between the actual heading angle and the desired LOS for the second trajectory and third trajectories, respectively.

From Figs. 5–7 presented above it can be seen that the convergence to the desired trajectory is done successfully and improved with the new method. This fact is more notorious in the second and third paths shown in Figs. 6 and 7, respectively, due to the required variation in the vehicle's speed. Moreover, the new method is very convenient and has the advantage of being adaptive, meaning that it is not necessary to establish a value for the distance n as in the previous method. It can be concluded that the new methodology presented here can be applied with success to minimize the error between the actual and the desired path of the vehicle as can be seen from Figs. 8 and 9.

7. Final remarks

In this paper a practical guidance and control system for an autonomous vehicle is introduced, using a way-point guidance algorithm based on LOS. An approach concerning the calculation of a dynamic LOS vector norm is presented in order to improve the convergence of the vehicle to the desired trajectory and turning the scheme independent of initial design value for the LOS distance (radius). Moreover, a PID heading controller including feedforward action and a speed controller obtained

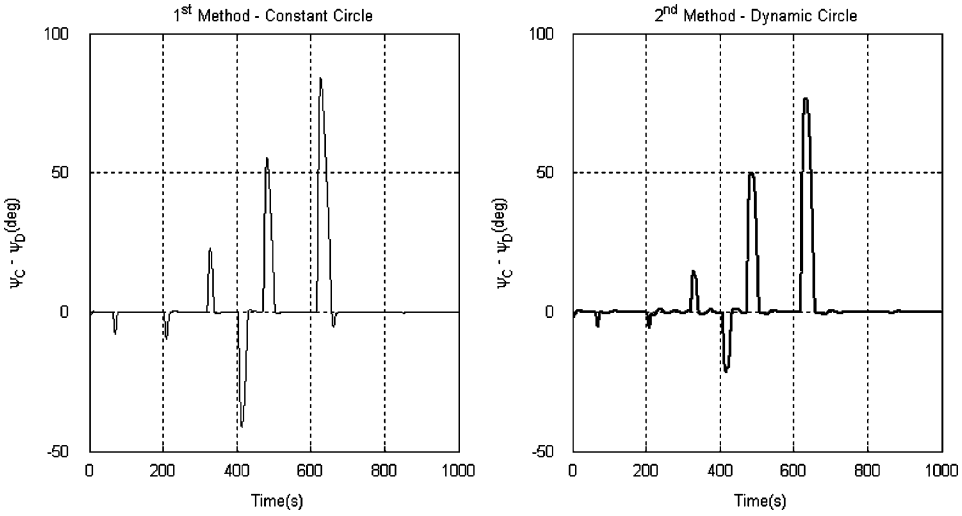

Fig. 8. Plot of the error ψ–ψ_d for the second simulated trajectory.

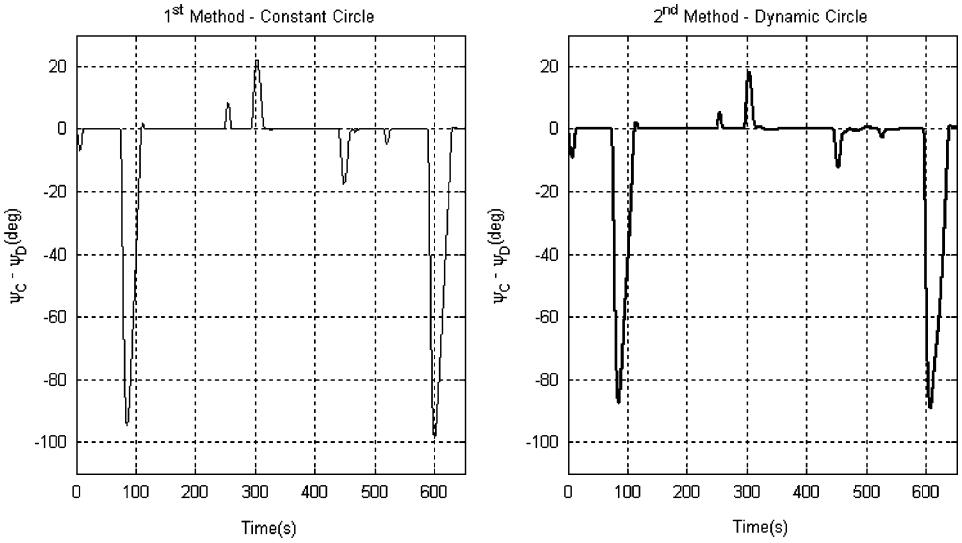

Fig. 9. Plot of the error ψ–ψ_d for the third simulated trajectory.

through state feedback linearization were developed. Simulation results based on the mathematical model of the ''Esso Osaka'' tanker are included to demonstrate the performance of the system. The presented approach can be readily applied to other vehicles or extended to higher dimensional control and guidance problems.

Acknowledgements

This is an extended version of the paper presented in 16th IFAC World Congress in Prague, Czech Republic, from July 4 to July 8, 2005. The first author has been financed by ''Fundação para a Ciencia e Tecnologia'' under Contract number SFRH/BD/6437/2001.

References

Abkowitz, M.A., 1980. Measurement of hydrodynamic characteristics from ship maneuvering trials by system identification. SNAME Transactions 88, 283–318.

BMT Fluid Mechanics Lda, 2001. Review of model testing requirements for FPSO's. Offshore Technology Report 2000/123, Teddington, United Kingdom.

Breivik, M., 2003. Nonlinear maneuvering control of underactuated ships. MSc thesis, Department of Engineering Cybernetics, Norwegian University of Science and Technology, Trondheim, Norway.

Breivik, M., Fossen, T.I., 2004a. Path Following of straight lines and circles for marine surface vessels. In: Proceedings of the Sixth IFAC CAMS, Ancona, Italy, pp. 65–70.

Breivik, M., Fossen, T.I., 2004b. Path following for marine surface vessels. In: Proceedings of the OTO'04, Kobe, Japan, pp. 2282–2289.

Clarke, D., 2003. The Foundations of Steering and Maneuvering. In: Proceedings of Sixth Conference on Maneuvering and control of marine crafts (MCMC'2003), Girona, Spain, pp. 2–16.

Fossen, T.I., 2000. Marine Control Systems: Guidance, Navigation and Control of Ships, Rigs and Underwater Vehicles (Marine Cybernetics AS). Trondheim, Norway.

Fossen, T.I., Breivik, M., Skjetne, R., 2003. Line-of-sight path following of underactuated marine craft. In: Proceedings of the Sixth IFAC conference on Maneuvering and Control of Marine Crafts (MCMC'2003), Girona, Spain, pp. 244–249.

Healey, A.J., Lienard, D., 1993. Multivariable sliding mode control for autonomous diving and steering of unmanned underwater vehicles. IEEE Journal of Oceanic Engineering 18 (3), 327–339.

Journée, J.M.J., 2001. A simple method for determining the manoeuvring indices k and t from zigzag trial data. DUT-SHL Technical. Report 0267, Delft, Netherlands.

McGookin, E.W., Murray-Smith, D.J., Lin, Y., Fossen, T.I., 1998. Ship steering control system optimization using genetic algorithms. Journal of Control Engineering Practice 8, 429–443.

Moreira, L., Guedes Soares, C., 2003. Dynamic model of maneuverability using recursive neural networks. Ocean Engineering 30 (13), 1669–1697.

Nomoto, K., Taguchi, T., Honda, K., Hirano, S., 1957. On the steering qualities of ships. Technical Report, International Shipbuilding Progress, 4.

Pettersen, K.Y., Lefeber, E., 2001. Way-point tracking control of ships. In: Proceedings of the 40th IEEE Conference on Decision and Control, Orlando, Florida USA, pp. 940–945.

SNAME, 1950. The Society of Naval Architects and Marine Engineers, Nomenclature for Treating the Motion of a Submerged Body Through a Fluid, Technical and Research Bulletin No. 1–5, 1950.